Optical routing and sensing with nanowire assemblies

Donald J. Sirbuly*†‡, Matt Law*†‡, Peter Pauzauskie*, Haoquan Yan*, Alex V. Maslov§, Kelly Knutsen*, Cun-Zheng Ning§, Richard J. Saykally*, and Peidong Yang*†¶

*Department of Chemistry, University of California, Berkeley, CA 94720; †Materials Sciences Division, Lawrence Berkeley National Laboratory, 1 Cyclotron Road, Berkeley, CA 94720; and §National Aeronautics and Space Administration Ames Research Center, MS 229-1, Moffett Field, CA 94035

The manipulation of photons in structures smaller than the wavelength of light is central to the development of nanoscale integrated photonic systems for computing, communications, and sensing. We assemble small groups of freestanding, chemically synthesized nanoribbons and nanowires into model structures that illustrate how light is exchanged between subwavelength cavities made of three different semiconductors. The coupling strength of the optical linkages formed when nanowires are brought into contact depends both on their volume of interaction and angle of intersection. With simple coupling schemes, lasing nanowires can launch coherent pulses of light through ribbon waveguides that are up to a millimeter in length. Also, interwire coupling losses are low enough to allow light to propagate across several right-angle bends in a grid of crossed ribbons. The fraction of the guided wave traveling outside the wire/ribbon cavities is used to link nanowires through space and to separate colors within multiribbon networks. In addition, we find that nanoribbons function efficiently as waveguides in liquid media and provide a unique means for probing molecules in solution or in proximity to the waveguide surface. Our results lay the spadework for photonic devices based on assemblies of active and passive nanowire elements and presage the use of nanowire waveguides in microfluidics and biology.

photonics | subwavelength | evanescent | nanoribbon | waveguide

Recently, our laboratories demonstrated the assembly of photonic circuit elements from SnO_2 nanoribbon and ZnO nanowire waveguides (1). High-aspect ratio nanoribbons/wires with diameters below the wavelength of light (typically 100–400 nm) were shown to act as excellent waveguides of both their own internally generated photoluminescence (PL) and nonresonant UV/visible light emitted from adjacent, evanescently coupled, nanowires. The length, flexibility, and strength of these single-crystalline structures enabled them to be manipulated and positioned on surfaces to create various single-ribbon shapes and multiribbon optical networks, including ring-shaped directional couplers and nanowire emitter-waveguide-detector junctions. This ability to control the shape of active and passive nanowire cavities provides a tool for investigating the cavity dynamics of subwavelength structures. Moreover, future advances in assembling the diverse set of existing nanowire building blocks (2) could lead to a novel and versatile photonic circuitry.

Here, we build on our initial demonstration of nanowire/ribbon photonic assembly with several proof-of-principle illustrations of optical routing between coupled nanowires. We first show that it is possible to deliver individual nanosecond light pulses from lasing GaN and ZnO nanowires through a ribbon waveguide, a prerequisite if nanowire photonic devices are to be useful in communications or computing applications. Simple networks of SnO_2 ribbons are then used to separate white light and route different colors based on a short-pass filtering effect. We also describe an optical crossbar grid made of two pairs of orthogonal ribbons that conducts light through abrupt 90° angles and provides a dramatic example of the nature of optical confinement in these subwavelength cavities. The fact that the waveguiding ability of our freestanding, flexible wires and ribbons survives in liquid media suggests a role for nanowire light delivery in microfluidics and biological sensing applications.

Materials and Methods

Single-crystalline SnO_2 nanoribbons were synthesized by using a chemical vapor transport process as described (3). SnO powder was placed in an alumina boat and heated in a tube furnace for 90 min at 1,100°C in flowing argon [300 torr (1 torr = 133 Pa), 50 standard cubic cm per min]. ZnO nanowires were grown as epitaxial arrays on sapphire substrates by the oxidation of metallic zinc at 800°C, using gold as a catalyst (4). The substrates were heated in a quartz tube for 30 min in flowing O_2/Ar. GaN nanowires were made by the chemical vapor transport of gallium metal in a quartz tube containing NH_3/H_2 and nickel-coated sapphire substrate (5). The tube was heated to 900°C for 4 h. The SnO_2 nanoribbons were dry-transferred en masse to oxidized silicon substrates (1 μm SiO_2, Silicon Sense, Nashua, NH). A triple-axis micromanipulator tipped with a tungsten probe (≈400-nm tip diameter) was used to remove individual ZnO and GaN nanowires from their growth substrates and deposit them with the ribbons.

Ribbons and wires were manipulated with the probe under a dark-field microscope. A HeCd laser (Melles Griot, Irvine, CA) provided unpolarized continuous wave resonant illumination (325 nm), whereas the fourth harmonic of a Nd:YAG laser (266 nm, 8 ns, 10 Hz) was used for pulsed pumping. Laser diodes (652 and 532 nm) and the HeCd laser (442 nm) supplied visible light for the filtering and fluorescence demonstrations. The lasers were focused to a beam diameter of ≈50 μm, giving a continuous wave power density of ≈175 W/cm² and a pulsed energy density of 1–100 μJ/cm². Spectra were acquired with a fiber-coupled spectrometer (gratings at 150 and 1,200 grooves per mm, SpecraPro 300i, Roper Scientific, Trenton, NJ) and liquid N_2-cooled charge-coupled device setup. Black-and-white and color images were recorded with two microscope-mounted charge-coupled device cameras (CoolSnap fx and CoolSnap cf, Photometrics, Tucson, AZ).

Propagation loss measurements were performed on individual SnO_2 nanoribbons dispersed on silica (n = 1.45) by using a commercial near-field optical microscope (NSOM) setup (Lumina, TopoMetrix) operating in collection mode. The NSOM probe (an etched single-mode optical fiber) was held fixed over the emission end of a ribbon (with a length >500 μm) while the UV laser spot was scanned along its length in ≈50-μm increments. Propagation losses were calculated from the resulting plots of intensity versus pump-probe separation assuming constant insertion losses (reasonable for the PL-generation scheme used here). We determined the coupling efficiency between nanoribbons by comparing the output intensity of two ribbon waveguides before and after an optical junction was formed between them.
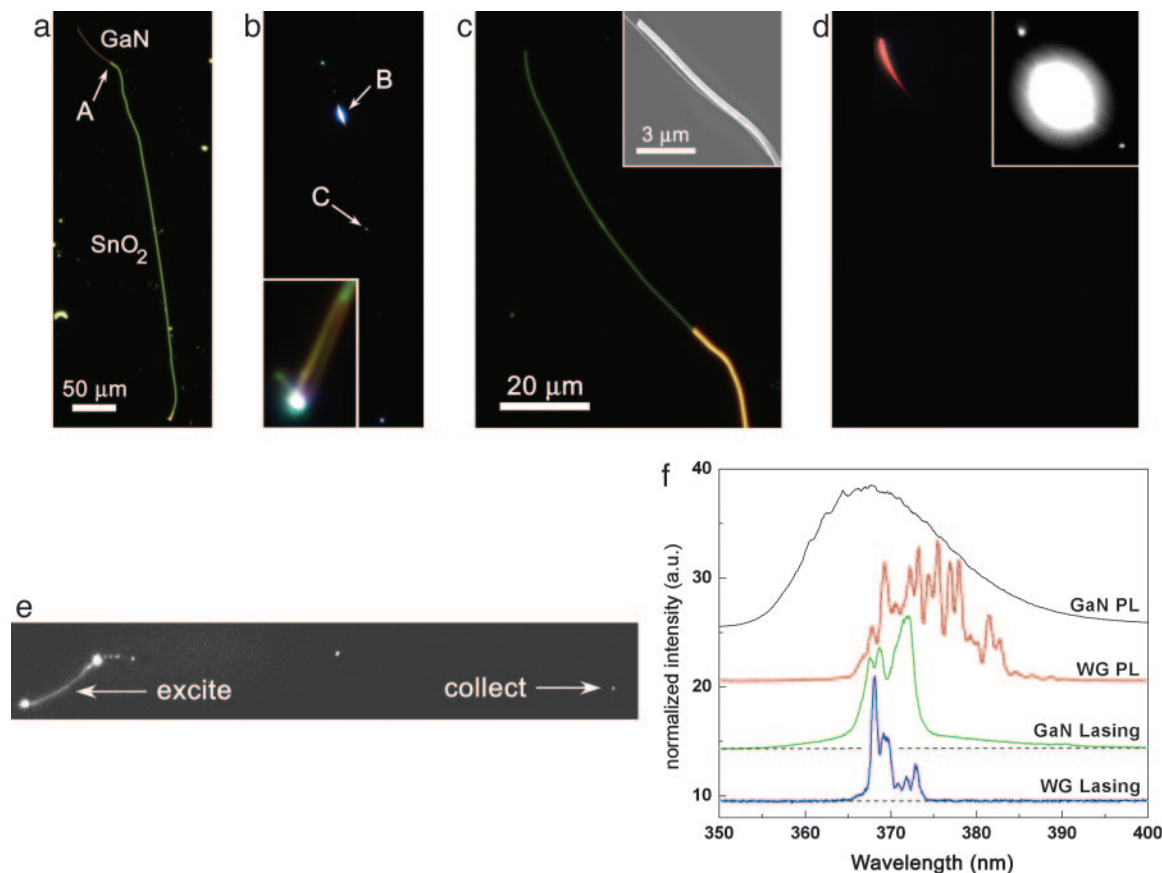

Fig. 1. The routing of GaN PL and lasing emission. (*a*) A dark-field optical image of a coupled GaN wire and SnO$_2$ ribbon. A denotes the location of the junction. (*b*) The same view as in *a*. Direct excitation of the SnO$_2$ ribbon at location B generates white PL that is guided to the ends of the SnO$_2$ cavity. Some of the light is scattered by a large particle found at C. (*Inset*) A zoomed view of the ribbon emission. (*c*) A magnified view of the junction area. (*Inset*) A scanning electron microscopic image showing that the two cavities are staggered over a distance of 9 μm and touch for $\approx$2 μm. (*d*) The same view as in *c*. Here, direct continuous wave excitation of the GaN wire generates UV band-edge emission at 365 nm and a small amount of visible defect emission at 650 nm. The cavity is too thin to permit the confinement of the red light, but (*Inset*) a UV camera detects strong waveguiding of the UV PL. (*e*) A magnified ($\times$1.5) optical image of *a* showing the routing of UV laser pulses from wire to ribbon. The GaN cavity was pumped above its lasing threshold by a pulsed 266-nm source (itself invisible to this detector). (*f*) Spectra comparing the GaN PL and lasing emission before and after passage through the ribbon cavity. The broad spontaneous emission peak (top) is broken into a series of sharp modes during its transit through the ribbon (WG PL). Likewise, the lasing emission at moderate pump power, which shows multiple modes (GaN lasing), is severely modulated by the mode structure of the SnO$_2$ cavity (WG lasing). The redshift of the guided spectra is consistent with band-edge absorption by SnO$_2$ below $\approx$365 nm. Spectra are normalized and offset for clarity.

Many of the ribbons/wires described in this article operate as single-mode fibers for certain experimental wavelengths, whereas others are multimode. For reference, the approximate single-mode cutoff diameters of a cylindrical step-index fiber in air are 140 nm (λ = 365 nm) and 265 nm (λ = 600 nm) for SnO$_2$, 112 nm (λ = 365 nm) for GaN, and 140 nm (λ = 380 nm) and 220 nm (λ = 510 nm) for ZnO (6). Ribbon and wire sizes were determined with a scanning electron microscope.

In the liquid experiments, droplets ($\approx$5 μl) of water or various alcohols were transferred to the oxide surface by pipette. The solvent droplets were then diced into smaller volumes (as small as 10 femtoliters) and positioned on the surface by using the manipulator.

Results and Discussion

Figs. 1 and 2 document several experiments that were performed with a single ribbon in various combinations with GaN and ZnO nanowires. Fig. 1*a* shows a GaN nanowire (130 nm in diameter $\times$ 65 μm in length) that was coupled to the SnO$_2$ nanoribbon (240 nm $\times$ 260 nm $\times$ 460 μm) with the micromanipulator. A magnified scanning electron microscopic view of the GaN–SnO$_2$ junction (Fig. 1*c*, *Inset*) indicates that the two structures are in

physical contact over a distance of $\approx$2 μm. This staggered-bonded configuration provides good optical coupling between the cavities and some degree of interwire adhesion (via electrostatic forces), which aids in the construction of multiwire networks. Typical power transfer efficiencies of $\approx$50% were measured for nanoribbons of similar size linked in a staggered geometry. These measurements also represent an upper bound on the coupling efficiency between ZnO or GaN wires and SnO$_2$ ribbons, which should show slightly lower efficiencies because of the mismatch in refractive index, size, and cross-sectional shape between wires and ribbons. We found that this staggered geometry did not cause appreciable scattering of light at the ribbon-ribbon interface. Therefore, the fraction of the guided power not transferred from wire/ribbon to ribbon is lost at the end facets of the primary waveguide. We have also tested several alternative coupling geometries. Butt-end coupling is less effective than staggered coupling because the emission from these subwavelength waveguides is poorly collimated. If two ribbons are crossed instead of staggered, the coupling losses decrease with shallower intersection angles, which has also been observed recently for crossed CdS nanowires (7). It is also possible to detect the transfer of light between ribbons that are weakly
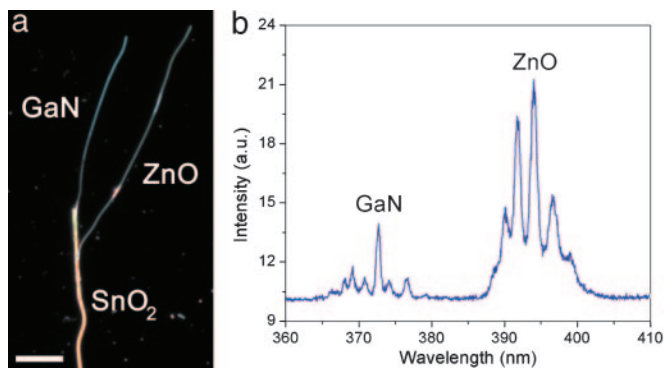
Fig. 2. Multilaser waveguiding. (*a*) Dark-field image of a GaN and a ZnO nanowire coupled to the same nanoribbon. (Scale bar: 10 μm.) (*b*) Spectrum of guided light collected at the far end of the ribbon when both wires were pumped above their lasing thresholds by the same train of optical pulses. This ribbon is also used in Figs. 1 and 6.

Fig. 3. Color filtering in a nanoribbon network. (*a*) Dark-field image of a four-ribbon assembly as it guides white PL generated at the pump spot (left) and separates it into a different color at the end of each ribbon (right). (Scale bar: 50 μm.) (*b*) Magnified view of the emission region. The branch ribbons 1–3 emit green, aqua, and blue light because of their progressively smaller cross sections (350 × 140 nm, 260 × 175 nm, and 210 × 135 nm, respectively). Their 50% cutoff wavelengths were determined by near-field scanning optical microscopy to be 543, 502, and 478 nm. The stem ribbon is 260 nm × 240 nm × 390 μm. (*c*) Nonresonant blue light is transmitted to the end of all four ribbons, whereas (*d*) green light is much more strongly guided by ribbon 1 than by ribbon 3 and (*e*) red light is filtered out by all three branches. (Scale bar for *b–e*: 20 μm).

linked across an air gap of up to several hundred nanometers (data not shown).

To demonstrate the routing of continuous wave light, we excited the GaN nanowire with the focused beam of a HeCd laser operating at 325 nm. Band-edge PL from the GaN cavity was channeled through the SnO_2 ribbon to emerge primarily at its far end. A fraction of the light was also scattered by imperfections along the length of the ribbon (i.e., attached particles or macroscopic step edges). Propagation losses through nanoribbons of this size are ≈10 dB/cm for wavelengths from 400 to 550 nm (smaller ribbons show higher losses of up to 80 dB/cm at 475 nm). Far-field spectra collected from the output end of the ribbon (Fig. 1*f*) show that the broad PL band of GaN is imprinted with the mode structure of the SnO_2 cavity during its transit. This mode structure is not longitudinal (Fabry-Perot) in nature, as it is for shorter nanowires (8); instead, it is likely caused by transverse modes that depend on ribbon shape and cross-sectional dimensions.

By pumping the GaN wire above its lasing threshold (≈100 μJ/cm^2, see Fig. 6, which is published as supporting information on the PNAS web site) with pulsed UV excitation, we were able to send single optical pulses from the nanowire laser through the nanoribbon waveguide (Fig. 1*e*). The spectrum of several thousand accumulated pulses (Fig. 1*f*) shows a series of sharp modes with a full width at half of maximum of 0.8 nm. These are the Fabry-Perot type lasing modes of the GaN wire resonator, modulated in intensity by the ribbon cavity. We have obtained similar results with junctions between ribbons and lasing ZnO nanowires. Moreover, it is possible to simultaneously guide the output of two (or more) nanolasers by coupling multiple ZnO and GaN wires to the same ribbon (Fig. 2), establishing the possibility of performing all-nanowire nonlinear wave mixing within single nanocavities. This is experimental verification that coherent optical pulses can be directly transferred between nanowires and steered hundreds of micrometers from their source. With high-frequency electrical pumping, nanowire laser/waveguide combinations could be used to transduce and shuttle packets of electro-optical information within future computing and communications devices.

Because diffraction losses in a subwavelength cavity increase markedly with wavelength, a ribbon waveguide preferentially confines the bluer portion of any nonmonochromatic beam. As a result, ribbons act as short-pass filters with cutoff wavelengths that are determined by their cross-sectional dimensions and overall length. We assembled a simple network consisting of four ribbons of different sizes to show how such a structure may be used to separate colors (Fig. 3). When excited at 325 nm, the
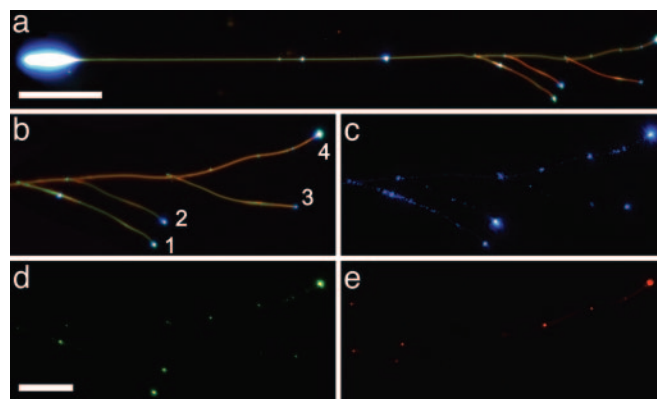
large ribbon that forms the stem of the network emits white light composed of two broad SnO_2 PL bands centered at 495 and 590 nm (Fig. 7, which is published as supporting information on the PNAS web site). Varying amounts of the stem emission then flows into the three shorter and consecutively thinner branch ribbons, separating the white light into green, aqua, and blue components (ribbons 1–3). Alternatively, monochromatic red light launched into the stem was effectively guided only by the stem ribbon, whereas green light was guided strongly (weakly) by the largest (smallest) branch and blue light passed through all four channels (Fig. 3 *b–e*). Although this color filtering effect works only in short-pass mode, and so cannot, for instance, isolate the pure red component of a white beam, it may prove useful in tasks such as providing local excitation for fluorophores with narrow absorption bands, such as quantum dots.

To test the limits of intercavity optical coupling, we assembled four nanoribbons into a rectangular grid (46 μm long × ≈25 μm wide) featuring X-junction vertices with small contact areas (<0.15 μm^2) (Fig. 4*a* and *Inset*). The structure was designed with one long channel for light input and seven short output channels that could be monitored simultaneously. As shown in Fig. 4*b*, direct excitation of the input channel triggered emission from all seven of the ribbon outputs, with the following intensity distribution: 1 ≫ 6 > 4 ≈ 7 > 3 > 5 > 2. This sequence is exactly the one we would expect after considering the trajectory of the incoming light and the intensity of scattering at the four ribbon-ribbon junctions. The light trajectory is important here because the low reflectivity of their end facets makes ribbons poor resonators (with an ideal finesse of ≈1.3). As such, most photons do not make multiple passes and light flow is highly directional. The right-angle intersections present significant obstacles to intercavity waveguiding by total internal reflection. At the same time, they act as quasi-isotropic scatterers that feed light between ribbons. Ribbon-to-ribbon losses, although nearly maximized in this geometry (<5% coupling efficiency), are still low enough for the activation of channels 2 and 3, which require photons to negotiate two right-angle junctions and transit three separate cavities. When we added a ZnO nanowire laser to the input channel and used it to launch light into the grid, emission was
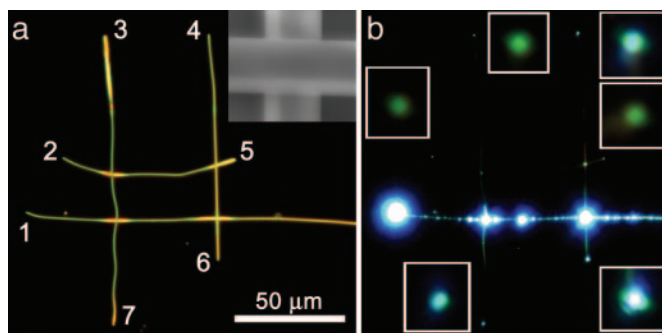
Sirbuly *et al.*

Fig. 4. Optical routing in a rectangular nanoribbon grid. (*a*) Dark-field image of the four-ribbon structure, with the input channel extending off the frame to the right and the output channels labeled 1–7. The ribbons vary in size from 300 to 400 nm on a side. (*Inset*) A scanning electron microscopic image of the junction at the lower right vertex. (*b*) PL image as the input channel is pumped at 325 nm. PL is guided to the seven output ends with different intensities as described in the text. Magnification is the same as in *a*. (*Insets*) Magnified (×4) views of output channels 2–7.

detected from all channels but 2 and 3; the number of injected photons was simply too small to illuminate the parallel ribbon in this case. Nanowire grids have already been used to implement rudimentary electronic logic (9). Integrated optical logic (10–12) and all-optical switching (13, 14) present exciting prospects, and our results show that grids of nanowires should be capable of routing signals for such tasks.

Because of their high refractive indices ($n \geq 2$), the nanoribbons and wires described here function well as waveguides in water and other liquids. This is a considerable advantage over subwavelength silica waveguides (15), which cannot efficiently confine visible light in liquids because of a low dielectric contrast ($n_{silica} \approx 1.45$). Waveguiding in liquids is especially important for integrated on-chip chemical analysis and biological spectroscopy in which small excitation and detection volumes are required. Fig. 8, which is published as supporting information on the PNAS web site, shows that the guided PL spectrum of a thin ribbon (in this case, 365 nm × 105 nm × 265 μm) resting on the oxide surface broadens to longer wavelengths when it is covered by pure water. Such a redshift would be anomalous for a fiber with a cladding of homogeneous refractive index, where one expects the replacement of air ($n = 1$) by water ($n = 1.33$) to increase losses and result in a blueshift of the mode cutoff. However, when a slab or strip waveguide exists in an asymmetric cladding environment (that is, when $n_{waveguide} > n_{subtrate} > n_{cover}$), as it does here, raising the index of the cover reduces its asymmetry with the substrate and improves confinement (16, 17). Numerical simulations show an increase in the effective guide index with a decrease in substrate-cover index profile, strongly supporting this view (see Fig. 9, which is published as supporting information on the PNAS web site). We note that the spectra of ribbons too thick to show a PL cutoff in air were unaffected by immersion in water.

Ribbon waveguides can sense molecules, proteins, or larger biological entities in solution by means of either an emission or absorption mechanism. In the former, a ribbon provides local excitation for fluorophores passing through the cone of scattered light at its output end, and the emission is collected by a fiber or microscope. To demonstrate this fluorescence scheme, we embedded the tip of a ribbon in a ≈3-pL droplet of 1 mM Silosuper Pink B [i.e., Rhodamine 6G (R6G) laser dye] in 1,5-pentanediol ($n = 1.45$). Blue light (442 nm) launched into the far end of the ribbon resulted in strong fluorescence from within the droplet, where the R6G emission mapped out the spatial intensity distribution of the waveguide output as a cone of light (Fig. 5a

and *Insets*). A fraction of this fluorescence was captured by the ribbon cavity and guided back to its far end, demonstrating that these waveguides are capable of routing signals both to and from liquids. Spectra acquired from both ends of the ribbon are presented in Fig. 5b. The guided fluorescence is red-shifted and somewhat sculpted by its passage through the ribbon, but there is little trace of the heavy mode imprinting evident, for instance, in Fig. 1f.

Fig. 5a also shows strong fluorescence originating from the segment of the ribbon wet by the droplet through capillary action. Here, dye molecules in proximity to the ribbon surface are excited in a subwavelength version of total internal reflection fluorescence (TIRF). In normal TIRF, excitation of a macroscopic waveguide (such as a microscope coverslip) generates an evanescent field of light that decays exponentially with distance from the waveguide surface, limiting the depth of excitation to a distance of ≈100 nm and enabling the local probing of structures such as cell membranes (18, 19). Evanescent wave sensing has also been demonstrated by using conventional optical fibers (20, 21). Because subwavelength fibers can carry a larger fraction of their modal power outside of the core, they enhance the intensity of this evanescent field and increase its penetration depth into the surroundings, making proportionally more power available to excite nearby molecules. Calculations indicate that ≈15% of the electric field intensity exists outside of the ribbon for the wavelength of light used in this experiment. In this case, the radial field intensity decays to 10% of its maximum value by ≈135 nm into the liquid solution. Because TIRF detection sensitivity scales with the fractional power present in the waveguide cladding, 1D nanostructures are promising waveguides for local fluorescence sensing using this approach.

A second way that nanoribbons/wires may be used for optical detection in solution relies on producing an absorption spectrum of molecules located on and near the ribbon surface. Absorbance detection, while inherently less sensitive than fluorescence methods, is applicable to a wider range of molecules and avoids the complications of fluorescent tagging. We launched white PL down a long ribbon (260 nm × 240 nm × 540 μm) onto the midpoint of which a ≈1-pL droplet of 1 mM R6G ($\alpha_{max} = 535$ nm) was deposited. Dye molecules in the droplet imprinted their absorption signature onto the propagating double-Gaussian beam, completely quenching transmission through the ribbon around the R6G absorption maximum (Fig. 5d). Considering the dye concentration, droplet size, and spatial extent of the evanescent field, we estimate that <40 attomoles of dye (≈24 million molecules) were probed in this experiment. Because this absorbance approach also uses the evanescent fraction of the guided field, smaller ribbons should again provide greater sensitivity. Other options for improvement include altering the cavity shape to increase the probe length, functionalizing the ribbon surface for selective biosensing, and launching multiple wavelengths for the simultaneous detection of analytes with different electronic transitions. The next steps are to integrate subwavelength nanoribbons/wires into microfluidic devices (22) and apply them as flexible probes in the study of live cells (23).

Conclusions

Chemically synthesized nanoribbon and nanowire waveguides have two unique and potentially useful features for subwavelength photonics applications. (*i*) Nanowires push subwavelength optical fibers beyond silica. The scores of materials that can now be made in nanowire form include active, passive, nonlinear, and semiconducting inorganic crystals, as well as a wide variety of polymers. Simultaneous manipulation of photons and charge carriers is possible within and between nanowires of different compositions. Also, many of these materials have higher refractive indices than silica-based glasses, permitting
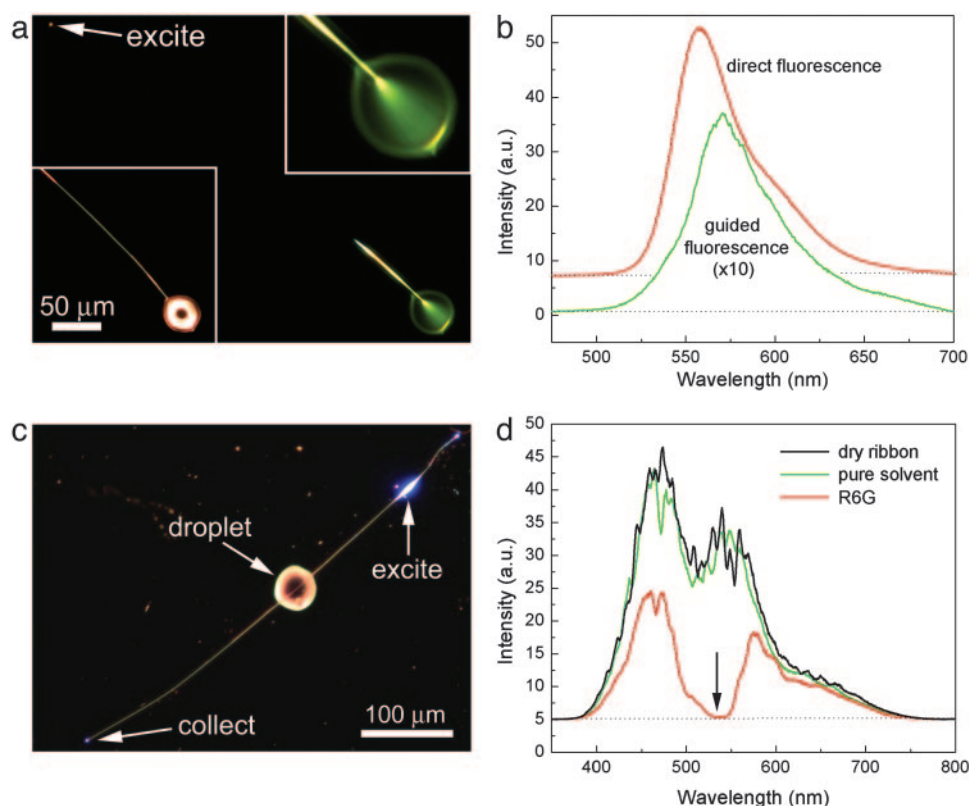
Fig. 5. Fluorescence and absorbance detection of R6G with a ribbon cavity. (*a*) Fluorescence image of a droplet of 1 mM R6G in 1,5-pentanediol excited by blue light from a ribbon waveguide (240 nm × 260 nm × 540 μm). The nanoribbon crosses the frame from upper left to lower right. A notch filter was used to block the excitation light. (*Left Inset*) A dark-field image showing the droplet and the bottom half of the ribbon. (*Right Inset*) A magnified (×2.5) view of the droplet emission, showing the light cone and evanescent pumping of the dye along the ribbon length. (*b*) Spectra taken of the droplet region (direct) and the fluorescence coupled back into the ribbon (guided). The redshift of the guided emission is a microcavity effect (see ref. 29). (*c*) Dark-field image of the ribbon with a droplet deposited near its middle (absorbance geometry). The ribbon was UV-pumped on one side of the droplet and probed on the other side as indicated. (*d*) Spectra of the guided PL without liquid present and with droplets of pure 1,5-pentanediol and 1 mM R6G. Losses caused by the presence of the pure solvent droplet were negligible. The arrow indicates the absorption maximum of R6G.

light of a given wavelength to be confined within thinner structures for denser integration. This strong confinement enables waveguiding in liquids and makes it possible to extend subwavelength guiding to telecommunications wavelengths using, for instance, ≈300-nm diameter Si or GaP wires (24, 25). (*ii*) Nanowires are freestanding, mechanically flexible elements that can be manipulated on surfaces or used as mobile probes in fluids. As such, they offer a type of versatility difficult to achieve with lithographically defined structures that are permanently affixed to their substrates.

The disadvantages of nanowire photonics include (*i*) the paucity of parallel assembly methods for accurately arranging large groups of nanowires into useful structures; (*ii*) relatively high interwire coupling losses compared with monolithic waveguides formed by lithography [coupling losses could be greatly reduced if branched, multicomponent nanowires were developed to replace the staggered or crossed nanowire cavities used here (26–28)]; and (*iii*) the lesser geometric perfection of nanowire assemblies relative to the precise shapes and sizes definable with lithography. Geometric imprecision introduces some uncertainty in the resulting light propagation and adds complexity to nanowire experiment/theory comparisons. Despite these limitations, we believe that freestanding, chemically synthesized nanowires represent a unique materials platform for the study and implementation of subwavelength optics.

1. Law, M., Sirbuly, D. J., Johnson, J. C., Goldberger, J., Saykally, R. J. & Yang, P. (2004) *Science* **305,** 1269–1272.
2. Law, M., Goldberger, J. & Yang, P. (2004) *Annu. Rev. Mater. Res.* **34,** 83–122.
3. Pan, Z. W., Dai, Z. R. & Wang, Z. L. (2001) *Science* **291,** 1947–1949.
4. Huang, M., Mao, S., Feick, H., Yan, H. Q., Wu, Y. Y., Kind, H., Weber, E., Russo, R. & Yang, P. (2001) *Science* **292,** 1897–1899.
5. Johnson, J. C., Choi, H.-J., Knutsen, K. P., Schaller, R. D., Yang, P. & Saykally, R. J. (2002) *Nat. Mater.* **1,** 106–110.
6. Snyder, A. W. & Love, D. (1983) *Optical Waveguide Theory* (Kluwer, Boston).
7. Barrelet, C. J., Greytak, A. B. & Lieber, C. M. (2004) *Nano Lett.* **4,** 1981–1985.
8. Johnson, J. C., Yan, H. Q., Yang, P. & Saykally, R. J. (2003) *J. Phys. Chem. B* **107,** 8816–8828.
9. Huang, Y., Duan, X., Cui, Y., Lauhon, L. J., Kim, K.-H. & Lieber, C. M. (2001) *Science* **294,** 1313–1317.
10. Tominaga, J., Mihalcea, C., Buchel, D., Fukuda, H., Nakano, T., Atoda, N., Fuji, H. & Kikukawa, T. (2001) *Appl. Phys. Lett.* **78,** 2417–2419.
11. O'Brien, J. L., Pryde, G. J., White, A. G., Ralph, T. C. & Branning, D. (2003) *Nature* **426,** 264–267.
12. Christodoulides, D. N., Lederer, F. & Silberberg, Y. (2003) *Nature* **424,** 817–823.
13. Ibrahim, T. A., Cao, W., Kim, Y., Li, J., Goldhar, J., Ho, P. T. & Lee, C. H. (2003) *IEEE Photon. Technol. Lett.* **15,** 36–38.

14. Almeida, V. R., Barrios, C. A., Panepucci, R. R. & Lipson, M. (2004) *Nature* **431,** 1081–1084.
15. Tong, L., Gattass, R. R., Ashcom, J. B., He, S. L., Lou, J. Y., Shen, M. Y., Maxwell, I. & Mazur, E. (2003) *Nature* **426,** 816–819.
16. Kogelnik, H. & Ramaswamy, V. (1974) *Appl. Opt.* **13,** 1857–1862.
17. Wakita, K. (1998) *Semiconductor Optical Modulators* (Kluwer, Boston).
18. Sund, S. E. & Axelrod, D. (2000) *Biophys. J.* **79,** 1655–1669.
19. Stephens, D. J. & Allan, V. J. (2003) *Science* **300,** 82–86.
20. Ruddy, V., MacCraith, B. D. & Murphy, J. A. (1990) *J. Appl. Phys.* **67,** 6070–6074.
21. Walczak, I. M., Love, W. F., Cook, T. A. & Slovacek, R. E. (1992) *Biosens. Bioelectron.* **7,** 39–48.
22. Petersen, N. J., Mogensen, K. B. & Kutter, J. P. (2002) *Electrophoresis* **23,** 3528–3536.
23. de Lange, F., Cambi, A., Huijbens, R., de Bakker, B., Rensen, W., Garcia-Parajo, M., van Hulst, N. & Figdor, C. G. (2001) *J. Cell Sci.* **114,** 4153–4160.
24. Tong, L., Lou, J. & Mazur, E. (2004) *Opt. Exp.* **12,** 1025–1035.
25. Schuurmans, F. J. P., Vanmaekelbergh, D., van de Lagemaat, J. & Lagendijk, A. (1999) *Science* **284,** 141–143.
26. Yan, H., He, R., Johnson, J. C., Law, M., Yang, P. & Saykally, R. J. (2003) *J. Am. Chem. Soc.* **125,** 4728–4729.
27. Dick, K. A., Deppert, K., Larrson, M. W., Martensson, T., Seifert, W., Wallenberg, L. R. & Samuelson, L. (2004) *Nat. Mater.* **3,** 380–384.
28. Wang, D., Qian, F., Yang, C., Zhong, Z. & Lieber, C. M. (2004) *Nano Lett.* **4,** 871–874.
29. Bulović, V., Khalfin, V. B., Gu, G., Burrows, P. E., Garbuzov, D. Z. & Forrest, S. R. (1998) *Phys. Rev. B* **58,** 3730–3740.

APPLIED PHYSICAL SCIENCES